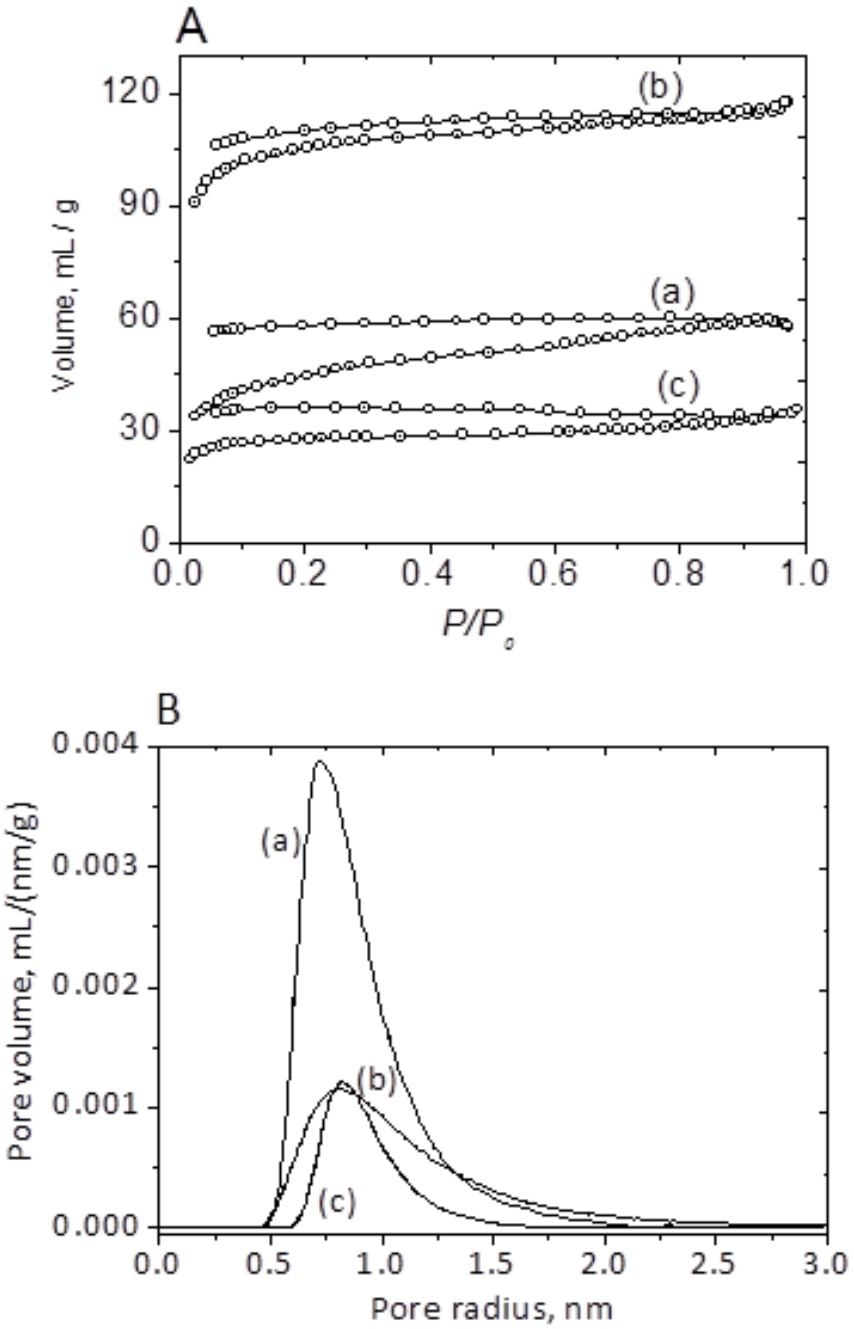

Figure 1. *(A) Nitrogen adsorption-desorption on the surface of electrodes (B) Pore size distribution for* ***(a)*** *CCP,* ***(b)*** *CCPHNO3 and* ***(c)*** *CCPWOT.*

Table 1 shows the changes in surface area, pore volume, and surface functional groups as a result of oxidation treatments. CCPHNO3 had the highest BET surface (337.1 $m^2 g^{-1}$), and a total pore volume measured at P/P_0 = 0.95 of 0.185 $cm^3 g^{-1}$, most of the pores being micropores (81.50 %), with an average pore width of 1.1 nm. On the other hand, CCPWOT exhibited the lowest BET surface (88.800 $m^2 g^{-1}$), with a much lower total pores volume (0.014 $cm^3 g^{-1}$) and a narrower pore width (1.408 nm). A pore size distribution in the range of micropore in which larger than the size of two solvated ions, was then identified as a way of improving the energy density and the power capability [11], whereas mesopores improved the ionic mass transport inside the bulk of carbon. Therefore, it was assumed that a good balance between micro- and mesoporosity was needed to maximize capacitance [12]. Some capacitance values from the literature are

provided to clarify the relationship between pore structure and capacitance. It can also be seen from the Table 1 that the some capacitance values obtained in this study are smaller than those obtained from the literatures.

Table 1. *Surface and electrochemical properties of the CCP, CCPHNO3 and CCPWOT electrodes.*

Electrode	S_{BET} / $m^2 g^{-1}$	V_{total} / $cm^3 g^{-1}$	micro pore content, %	Functional groups concentration, mmol g^{-1}				$C_{sp,max}$ F g^{-1}
				fenolic	lactonic	carboxylic	base	
CCP	149.848	0.093	56.249	0.200	3.85	0.00	0.24	1.22
CCPHNO3	337.116	0.185	81.499	0.100	3.08	0.20	0.19	27.68
CCPWOT	88.800	0.014	28.306	0.200	3.40	0.10	0.22	2.23
Carbon from sucrose [13]	2749.0	2.01						233
Carbon from sago waste [14]	1408.2	0.897						64.1
Carbon from coal [14]	179.2	0.073						16.2

S_{BET} – specific surface area; V_{total} - total pore volume, measured at P/P_0=0.995.

Furthermore, the specific surface area of the CCPHNO3 electrode as listed in Table 1 is 337.116 $m^2 g^{-1}$, which is higher than that of the CCP and CCPWOT electrode, *i.e.* 149.85 and 88.80 $m^2 g^{-1}$, respectively. The Boehm analysis reveals that the three electrodes have similar amounts of functional groups, except for the carboxylic and lactone groups. A computational study was undertaken on the effect of the two functional groups on the structure of graphite basal. The study found that the COOH functional groups that fill the vertical plane will bend graphite layer led to reduced effectiveness of electron transfer between layers. These functional groups improved capacitive processes of the carbon [15], and facilitated the penetration of the electrolyte ions into the interior pores. Although the CCPWOT electrode has many more functional groups, however, many more pores were vanished and the surface area was decreased, leading to a decrease in the capacitance of electrode. Furthermore, changes in the carbon pore structure can be clearly seen as surface morphology by using electron microscope.

The micrographs clearly indicate that the three electrodes have different surface morphologies. Figure 2a and 2d show the analysis of the CCP microstructure by SEM. They revealed continuous and smooth surface of the CCP with less grain boundaries wood (Figure 2a and 2d) due to the limited process of opening pore in line with the nature of the wood. The other SEM pictures show the opening pores in the surface of the carbon which occurred when CCP was treated with nitric acid (CCPHNO3), especially the oxidation of low molecular weight carbon. These SEM images of CCPHNO3 show irregular sizes and flaky grains in which the structures tend to form voids between the grains (Figure 2b and e). The number of grains and micropores of CCPHNO3 are higher than those of CCPWOT and CCP, due to the reaction between low molecular weight carbon fragments with nitrogen. The oxidation reaction generated volatile molecules that leave the pores behind after volatilization. Furthermore, SEM images of CCPWOT show more regular size and relatively uniform (Figure 2c and f). This porous structure, *i.e.* pore volume, surface area and pore size distribution along with functional groups on the surface of carbon are regarded as the important factors which determined the properties of capacitive processes, *i.e.* ionic accessibility, electrical double layer and redox reactions [16-18].

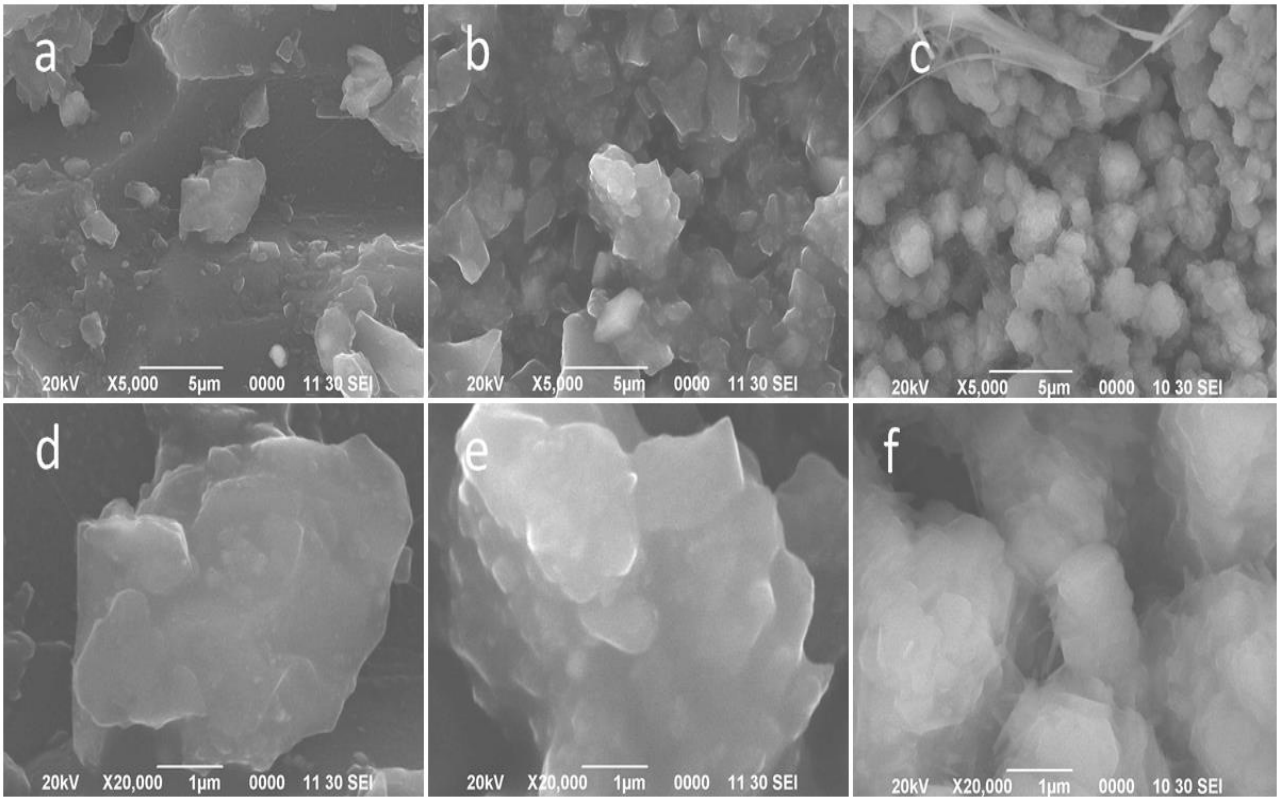

Figure 2. *SEM images for CCP* ***(a and d)****, CCPHNO3* ***(b and e)****, and CCPWOT* ***(c and f)***

Electrochemical performance

Cyclic voltammetry tests were conducted at scan rates of 2, 5, 10, 20, 50, and 100 mV s^{-1} with potential windows ranging from -1 to 1 V versus Ag/AgCl in 1, 2, and 4 mol L^{-1} KOH or H_2SO_4 aqueous solution to quantify the electrochemical performance of CCP, $CCPHNO_3$ and CCPWOT electrodes. As shown in Figure 3 and 4, no pronounced reversible reduction oxidation peak can be observed from voltammograms for the three electrodes. The shape of the voltammograms was different from one to another.

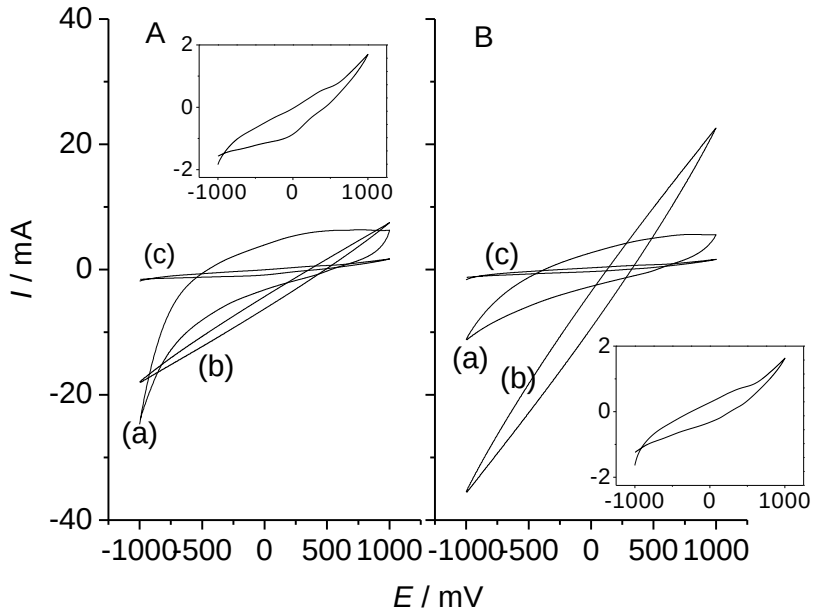

Figure 3. *CV Curve of carbon electrodes* ***(a)*** *CCP,* ***(b)*** *CCPHNO3 and* ***(c)*** *CCPWOT in the H_2SO_4 1M* ***(A)*** *and 4M* ***(B)****. Scan rate was 20 mV s^{-1}.* ***Inset****: magnification of voltammogram* ***(c)****.*

The voltammogram of the CCPWOT electrode was relativelylower compared to the other two curves. Therefore the oxidation treatment under water steam reduced the capacitance. On the other hand, the highest current of CCPHNO3 electrode points to the largest capacitance. The changes in capacitance occurred on the electrode after the oxidation process was associated with changes in pore volume of carbon, as previously described. Oxidation using strong acid clarified the existence of the Faraday process (redox reaction) that occurred at the carbon as described by other authors [19]. The voltammograms shape of CCPHNO3 in both acid and base electrolytes are much the same, which means that the tendency to establish a redox reaction was similar. The voltammogram area in Figure 3 shows the decrease in capacitance at high concentrations of H_2SO_4. By contrast, the capacitance of the electrodes increased at a low concentration KOH (Figure 4).

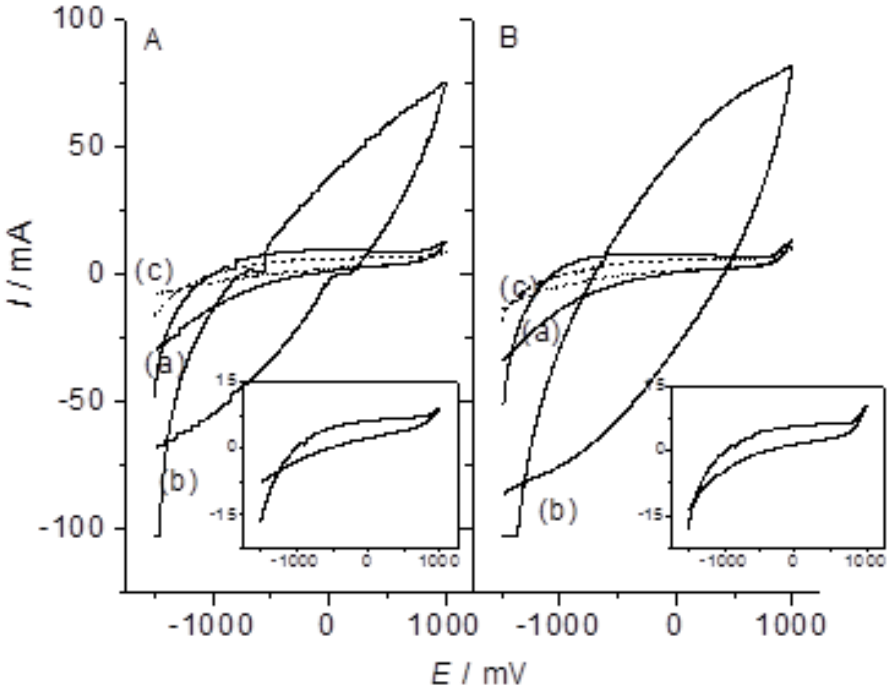

Figure 4. *Voltammogram of carbon electrodes* ***(a)*** *CCP,* ***(b)*** *CCPHNO3 and* ***(c)*** *CCPWOT in the KOH 2M* ***(A)*** *and 4M* ***(B)****. Scan rate was 5mV s-1.* ***Inset****: magnification of voltammogram* ***(c)****.*

Calculations of specific capacitances for all electrodes at various scan rates in the H_2SO_4 solution are presented in Figure 5. At the 5 mV s^{-1} scans rate in H_2SO_4, the CCP electrode had a specific capacitance of 1.2 F g^{-1}, while at a scan rate of 100 mV s^{-1} this was 0.22 F g^{-1}. Capacitance values of the CCPWOT electrode (Figure 5 B) at 5 – 10 mV s^{-1} were lower than that of CCP (Figure 5 A), but were higher at 20 – 100 mV s^{-1}. The capacitance values of CCP and CCPWOT electrodes were much smaller than those of the CCPHNO3 electrode (Figure 5 C). Maximum capacitance for non-oxidized, steam and acid oxidized electrodes were 1.22, 0.63 and 2.57 F g^{-1}, respectively. These values occurred at 5 mV s^{-1}.

Plots of the electrodes specific capacitances *vs*. scan rate in KOH are presented in Figure 6. Capacitances of CCP in KOH were much the same as those in H_2SO_4 both at low and high scan rates. Contrary to what occurred in the H_2SO_4, the capacitance values of the CCPWOT electrode (Figure 6B) were higher than those of CCP (Figure 6A), both at low and high scan rates. Capacitance values of CCP and CCPWOT electrodes were also much smaller than those of the CCPHNO3 electrode. Plot of specific capacitance of CCPHNO3 in KOH was discrete (Figure 6C) due to instability of the system, especially at a scan rate higher than 10 mV s^{-1}. A stable voltammogram

was only obtained at a scan rates higher than 40 mV s^{-1} at 1M KOH. Capacitance value for acid and steam oxidized electrodes were 2.23 and 27.68 F g^{-1}, respectively.

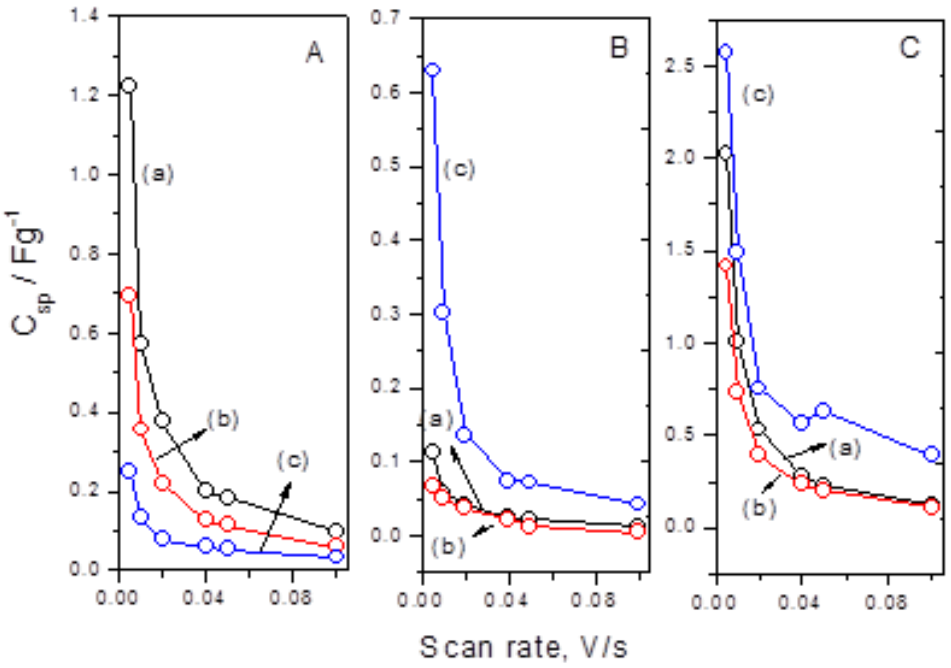

Figure 5. *Plot of specific capacitance of carbon electrode* ***(A)*** *CCP,* ***(B)*** *CPPWOT and* ***(C)*** *CCPHNO3 versus scan rate in H_2SO_4* ***(a)*** *4M,* ***(b)*** *2M and* ***(c)*** *1M.*

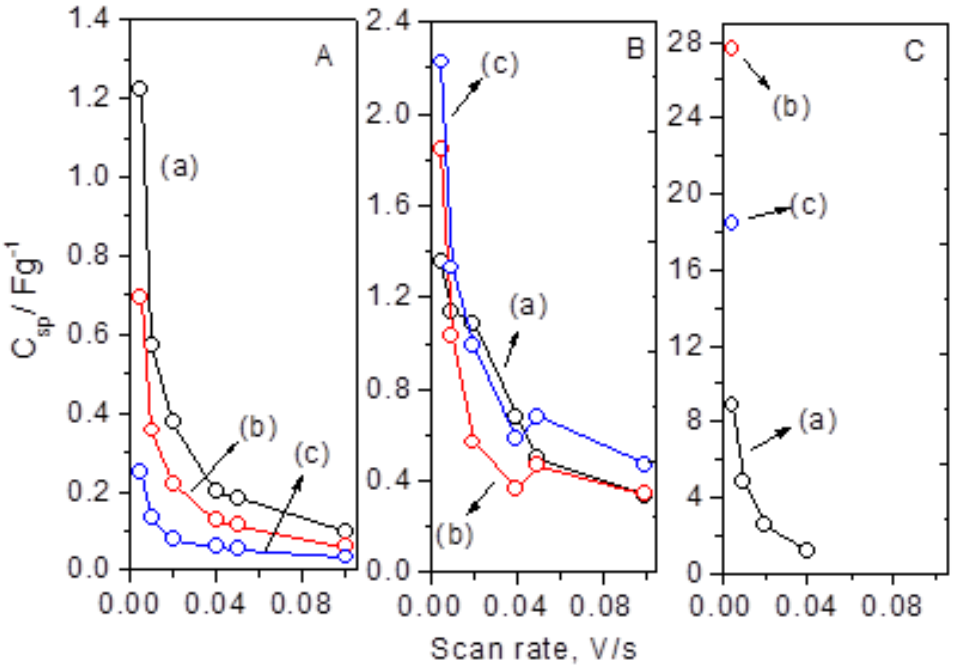

Figure 6. *Plot of specific capacitance (C_{sp})of carbon electrode* ***(A)*** *CCP,* ***(B)*** *CPPWOT and* ***(C)*** *CCPHNO3 versus scan rate in KOH* ***(a)*** *4M,* ***(b)*** *2M and* ***(c)*** *1M.*

The presence of the micropores in the activated carbon are unique for Gelam wood. Combining their uniqueness, simplicity of the preparation method and the abundance availability, makes these electrode materials relatively inexpensive and environmentally friendly. Thus Gelam wood activated carbon has the potential to be developed as electrodes in electrochemical capacitors.

Conclusions

The three types of electrodes, namely CCP, CCPHNO3 and CCPWOT, prepared from Gelam wood activated carbon, have different surface morphologies which basically contained many micropores. CCP has continuous - smooth surface and contains very few grain boundaries. On the other hand CCPWOT and CCPHNO3 have rough surfaces and contain many cracks. The different oxidation methods using nitric acid and water steam gave different effects on the surface area of the carbons. Acid nitric oxidation led to a larger pore volume and surface area, while water steam oxidation led the opposite effect. In addition, CCPHNO3 had relatively large amounts of micropores. The presence of surface oxides was important factor in improving the capacitance of electrode and increased the effective utilization of the pore structure. CCPHNO3 had the highest capacitance value of 27.68 F g^{-1} while the specific capacitance of the electrode CCPWOT was similar to CCP, at 2.23 and 1.22 F g^{-1}, respectively.

References

[1] M. Jayalakshmi, K. Balasubramanian, *Int. J. Electrochem. Sci*. **3** (2008) 1196−1217
[2] W. Li, H. Probstle, J. Fricke, *J. Non-Cryst. Solids* **325** (2003) 1−5
[3] A.G. Pandolfo, A.F. Hollenkamp, *J. Power Sources* **157** (2006) 11−27
[4] E. Taer, M. Deraman, I.A. Talib, A. Awitdrus, S.A. Hashmi, A.A. Umar, *Int. J. Electrochem. Sci*. **6** (2011) 3301 – 3315
[5] C. Merino, P. Soto, E. Vilaplana-Ortego, J.M.G.d. Salazar, F. Pico, J.M. Rojo, *Carbon* **43** (2005) 551−557
[6] H.P. Boehm, Carbon 32 (1994) 759-769
[7] C. Nieto-Delgado, M. Terrones, J.R. Rangel-Mendez, *Biomass Bioenerg.* **35** (2011) 103−112
[8] S. Villar-Rodil, A. Martinez-Alonso, J.A. Pajares, J.M.D. Tascon, M. Jasienko-Hałat, E. Broniek, J. Kaczmarczyk, A. Jankowska, A. Albiniak, T. Siemieniewska, *Micropor. Mesopor. Mat.* **64** (2003) 11-19
[9] K.P. Gadkaree, M. Jaroniec, *Carbon* **38** (2000) 983−993
[10] K. Ramakrishnan, C. Namasivayam, *Sustain. Environ. Res.* **19** (2009) 173 − 178
[11] C. Du, N. Pan, *Nanotechnology* **17** (2006) 5314−5318
[12] R. Nickolov, D. Kovacheva, M. Mladenov, N.Velichkova, R. Raicheff, P. Tzvetkova, *J. Univ. Chem. Tech. Metall.* **46** (2011) 275−282
[13] K. Xia, Q. Gao, J. Jiang, J. Hu, *Carbon* **46** (2008) 1718-1726
[14] H. Aripin, L. Lestari, D. Ismail, S. Sabchevski, *Open Mat. Sci. J.* **4** (2010) 117−124
[15] M.J. Bleda-Martınez, J.A. Macia-Agullo, D. Lozano-Castello, E. Morallon, D. Cazorla-Amoros, A. Linares-Solano, *Carbon* **43** (2005) 2677−2684
[16] L.L. Zhang, X. Zhao, H. Ji, M.D. Stoller, L. Lai, S. Murali, S. Mcdonnell, B. Cleveger, R.M. Wallace, R.S. Ruoff, *Energy Environ. Sci.* **5** (2012) 9618-9625
[17] B.G. Choi, Y.S. Huh, W.H. Hong, H.J. Kim, H.S. Park, *Nanoscale* **4** (2012) 5394-5400
[18] E. Frackowiak, F. Beguin, *Carbon* **39** (2001) 937-950
[19] M. Seredych, D. Hulicova-Jurcakov, G.Q. Lu, T.J. Bandosz, *Carbon* **46** (2008) 1475-1388